

Macroscopic Greenberger-Horne-Zeilinger and W states in flux qubits

Mun Dae Kim*

Korea Institute for Advanced Study, Seoul 130-722, Korea

Sam Young Cho[†]

*Center for Modern Physics and Department of Physics, Chongqing University, Chongqing 400044, People's Republic of China
and Department of Physics, The University of Queensland, Brisbane 4072, Australia*

(Received 19 December 2007; published 26 March 2008)

We investigate two types of genuine three-qubit entanglement, known as the Greenberger-Horne-Zeilinger (GHZ) and W states, in a macroscopic quantum system. Superconducting flux qubits are theoretically considered in order to generate such states. A phase coupling is proposed to offer enough strength of interactions between qubits. While an excited state can be the W state, the GHZ state is formed at the ground state of the three flux qubits. The GHZ and W states are shown to be robust against external flux fluctuations for feasible experimental realizations.

DOI: 10.1103/PhysRevB.77.100508

PACS number(s): 74.50.+r, 03.67.-a, 85.25.Cp

Entanglement plays a crucial role in quantum information science. Controllable quantum systems such as photons, atoms, and ions have provided the opportunities to generate the entanglements. Recent experiments on two qubits have shown the existence of entanglement in different types of *microscopic* systems. Further, multipartite entanglements such as the Greenberger-Horne-Zeilinger¹ (GHZ) and W (Refs. 2 and 3) states have been demonstrated in recent experiments of atoms,⁴ photons, and trapped ions.^{5,6} However, in solid-state qubits, it has not yet been achieved.

As a *macroscopic* quantum system, superconducting qubit systems have been investigated intensively in experiments because their system parameters can be controlled to manipulate quantum states coherently. Indeed, the entanglements between two charges,⁷ phase,^{8,9} and flux qubits^{10,11} have been reported. While the timely evolving states in the experiments of charge qubits⁷ exhibit a partial entanglement, the excited level (*eigenstate*) of capacitively coupled two phase qubits⁹ shows higher fidelity for the entanglement. The experiments in Ref. 10 show a possibility that two flux qubits can be entangled by a macroscopic quantum tunneling between two-qubit states, flipping both qubits. Actually, the higher fidelity in the capacitively coupled two phase qubits is caused by the two-qubit tunneling processes.⁹ In a very recent study, the two-qubit tunneling process was theoretically shown to play an important role in generating the Bell states, maximally entangled, in the ground and excited states.¹²

For multipartite entanglements in superconducting qubit systems, there have been few studies. To produce the GHZ state in three charge qubits, only a way of doing a local qubit operation via time evolutions was suggested.¹³ As one of the possible directions to produce such multipartite entanglements, then it is natural to ask how to create the W state as well as the GHZ state in the *eigenstates* of superconducting three-qubit systems. Here, we consider three flux qubits. Normally, the interaction strength between inductively coupled flux qubits¹⁴ is not so strong that the controllable range of interaction is not sufficiently wide. To control a wide range of interaction strengths in the qubits, we use the phase-coupling scheme¹⁵⁻¹⁹ for three qubit [see Fig. 1(a)] which enables one to generate the GHZ and W states and to

keep them robust against external flux fluctuations for feasible experimental realizations.

We start with the model shown in Fig. 1(a). The Hamiltonian is written by $\hat{H} = \frac{1}{2} \hat{P}_i^T M_{ij}^{-1} \hat{P}_j + U_{\text{eff}}(\hat{\phi})$, where $\hat{P}_i = -i\hbar \partial / \partial \hat{\phi}_i$ and $M_{ij} = (\Phi_0 / 2\pi)^2 C_i \delta_{ij}$ with the capacitance of the Josephson junctions C_i . The dynamics of the flux qubits²⁰ are described by the phase variables $\hat{\phi} = (\phi_{qi}, \phi'_q)$ with $q = a, b, c$ and $i = 1, 2, 3$, where ϕ 's are the phase differences across the Josephson junctions. If we neglect the small inductive energy, the effective potential is written in terms of the Josephson junction energies, $U_{\text{eff}}(\phi) = \sum_q [\sum_{i=1}^3 E_{Ji} (1 - \cos \phi_{qi}) + E'_j (1 - \cos \phi'_q)]$. The periodic boundary conditions involved in the qubit loops and the connecting loops can be written as

$$\phi_{q1} + \phi_{q2} + \phi_{q3} = 2\pi(n_q + f_q), \quad (1)$$

$$(\phi_{a1} - \phi_{c1}) - \phi'_a + \phi'_c = 2\pi r, \quad (2)$$

$$(\phi_{b1} - \phi_{c1}) - \phi'_b + \phi'_c = 2\pi s, \quad (3)$$

where $q = a, b$, and c is qubit index and r, s , and n_q integers. Here, $f_q \equiv \Phi_q / \Phi_0$ with external flux Φ_q and the superconducting unit flux quantum $\Phi_0 = h/2e$. Two independent conditions in Eqs. (2) and (3) are the boundary conditions for connecting loops. For simplicity, we consider $E_{J2} = E_{J3} = E_J$ and $C_2 = C_3 = C$, so we can set $\phi_{q2} = \phi_{q3}$ and Eq. (1) becomes $\phi_{q1} = 2\pi(n_q + f_q) - 2\phi_{q3}$. The results for $E_{J2} \neq E_{J3}$ are qualitatively the same.

At the coresonance point $(f_a, f_b, f_c) = (1/2, 1/2, 1/2)$, the effective potential is given by

$$U_{\text{eff}}(\phi) = \sum_{q=a,b,c} (E_{J1} \cos 2\phi_{q3} - 2E_J \cos \phi_{q3} - E'_j \cos \phi'_q) + 3E_{J1} + 6E_J + 3E'_j. \quad (4)$$

Here, we introduce a rotated coordinates $\tilde{\varphi} = (\phi_\alpha, \phi_\beta, \phi_\gamma)$ in Fig. 1(b). The Euler rotations provide new coordinates such as $\tilde{\varphi}^T = \mathcal{R}_2(\chi, 0, 0) \mathcal{R}_1(0, 0, \theta) \varphi^T = \mathcal{R}(\chi, \theta) \varphi^T$, with $\chi = -\tan^{-1} \sqrt{2}$, $\theta = -\pi/4$, and $\varphi = (\phi_{a3}, \phi_{b3}, \phi_{c3})$, which can be written explicitly as

$$\begin{pmatrix} \phi_\alpha \\ \phi_\beta \\ \phi_\gamma \end{pmatrix} = \frac{1}{\sqrt{6}} \begin{pmatrix} \sqrt{3} & -\sqrt{3} & 0 \\ 1 & 1 & -2 \\ \sqrt{2} & \sqrt{2} & \sqrt{2} \end{pmatrix} \begin{pmatrix} \phi_{a3} \\ \phi_{b3} \\ \phi_{c3} \end{pmatrix}. \quad (5)$$

In the same way, a new coordinates for $\boldsymbol{\varphi}' = (\phi'_a, \phi'_b, \phi'_c)$ is given as $\tilde{\boldsymbol{\varphi}}'^T = \mathcal{R}(\chi, \theta) \boldsymbol{\varphi}'^T$, with $\tilde{\boldsymbol{\varphi}}' = (\phi'_\alpha, \phi'_\beta, \phi'_\gamma)$. Using the boundary conditions of Eqs. (2) and (3), the Hamiltonian is written in the transformed coordinates, $\tilde{\boldsymbol{\phi}} \equiv (\phi_\alpha, \phi_\beta, \phi_\gamma, \phi'_\gamma)$, as $\hat{H} = \sum_{\mu=\alpha,\beta,\gamma} \frac{\hat{p}_\mu^2}{2M_\mu} + \frac{\hat{p}'_\gamma{}^2}{2M'_\gamma} + U_{\text{eff}}(\tilde{\boldsymbol{\phi}})$, where $M_\alpha = M_\beta = 4C_1 + 2C + 2C'$, $M_\gamma = 4C_1 + 2C$, and $M'_\gamma = C'$. Note that the value of ϕ'_γ is determined at the potential minimum, $\partial U_{\text{eff}}(\tilde{\boldsymbol{\phi}}) / \partial \phi'_\gamma = 0$.

The eight corners of the hexahedron in Fig. 1(b) correspond to the three-qubit states. Here, the $|\downarrow\rangle$ ($|\uparrow\rangle$) is defined as diamagnetic (paramagnetic) current state which corresponds to positive (negative) value of ϕ_{qi} in the boundary condition of Eq. (1). These states can be represented more clearly in the rotated coordinates $(\phi_\alpha, \phi_\beta, \phi_\gamma)$ because the effective potential $U_{\text{eff}}(\boldsymbol{\phi})$ has threefold rotational symmetry about the ϕ_γ axis, which can be shown as in the following. Using the transformation of Eq. (5), one of the terms in Eq. (4) is written as $\sum_{q=a,b,c} \cos \phi_{q3} = \cos(\phi_\gamma/\sqrt{3}) [2 \cos(\phi_\beta/\sqrt{6}) \cos(\phi_\alpha/\sqrt{2}) + \cos(2\phi_\beta/\sqrt{6})] - \sin(\phi_\gamma/\sqrt{3}) [2 \sin(\phi_\beta/\sqrt{6}) \cos(\phi_\alpha/\sqrt{2}) - \sin(2\phi_\beta/\sqrt{6})]$. Here, if we rotate the potential by $2\pi/3$ about the ϕ_γ axis as $\psi_\alpha = -(1/2)\phi_\alpha - (\sqrt{3}/2)\phi_\beta$, $\psi_\beta = (\sqrt{3}/2)\phi_\alpha - (1/2)\phi_\beta$, and $\psi_\gamma = \phi_\gamma$, we can easily check the invariance of the effective potential, $U_{\text{eff}}(\boldsymbol{\phi})$.

In order to study the GHZ state, $|\Psi_{\text{GHZ}}\rangle = (|\uparrow\uparrow\uparrow\rangle + |\downarrow\downarrow\downarrow\rangle)/\sqrt{2}$, we draw the yellow (dark gray) square introducing the auxiliary coordinates defined by $\phi_p \equiv (\phi_{a3} + \phi_{b3})/\sqrt{2}$ and $\phi_m \equiv (\phi_{a3} - \phi_{b3})/\sqrt{2}$, while for W state, $|\Psi_W\rangle = (|\uparrow\downarrow\downarrow\rangle + |\downarrow\uparrow\downarrow\rangle + |\downarrow\downarrow\uparrow\rangle)/\sqrt{3}$, we consider the blue (light gray) triangle. Figures 1(c)–1(e) show the effective potential $U_{\text{eff}}(\boldsymbol{\phi})$ in Eq. (4). When the three qubits are decoupled for $E'_j = 0$,^{15,17} Fig. 1(c) shows that the single-qubit tunneling t_1^a is dominant over the three-qubit tunneling t_3^a . As E'_j increases, it is shown in Fig. 1(d) that the three-qubit tunneling becomes dominant. Then, the GHZ state is expected to be formed at the ground state. The dotted line in Fig. 1(d) coincides with ϕ_γ axis in Fig. 1(b). Along the ϕ_γ axis, the double-well potential is given by $U_{\text{eff}}(0, 0, \phi_\gamma, \sqrt{3}\pi) = 3E_{J1}(1 + \cos \frac{2\phi_\gamma}{3}) + 6E_J(1 - \cos \frac{\phi_\gamma}{3})$, where the barrier height is proportional to E_{J1} . The WKB approximation allows us to calculate the three-qubit tunneling t_3^a through this double-well potential.^{21,22} Other tunnelings such as single-qubit tunnelings, t_1^a and t_1^b , and two-qubit tunnelings, t_2^a and t_2^b can also be calculated. The tight-binding approximation based on the eight states of three qubits gives the effective Hamiltonian, $H = \sum_{\nu, \nu'} E_{\nu\nu'} |\nu\rangle \langle \nu'| - \sum_{\nu, \nu', \nu''} t_{\nu\nu''} |\nu\rangle \langle \nu''|$, where $t_{\nu\nu''} = t_i^{a(b)}$ and $|\nu\rangle = |s_a s_b s_c\rangle$, with $s_q \in \{\uparrow, \downarrow\}$.

The global entanglement for tripartite systems can be quantified by the Q measure.²³ For a normalized arbitrary three-qubit state, $|\Psi\rangle = c_1 |\downarrow\downarrow\downarrow\rangle + c_2 |\downarrow\downarrow\uparrow\rangle + c_3 |\downarrow\uparrow\downarrow\rangle + c_4 |\uparrow\downarrow\downarrow\rangle + c_5 |\uparrow\downarrow\uparrow\rangle + c_6 |\uparrow\uparrow\downarrow\rangle + c_7 |\uparrow\uparrow\uparrow\rangle$, the Q factor is given by $Q(|\Psi\rangle) = 4/3 \sum_{j=1}^3 D_j(|\Psi\rangle)$, where $D_1(|\Psi\rangle)$

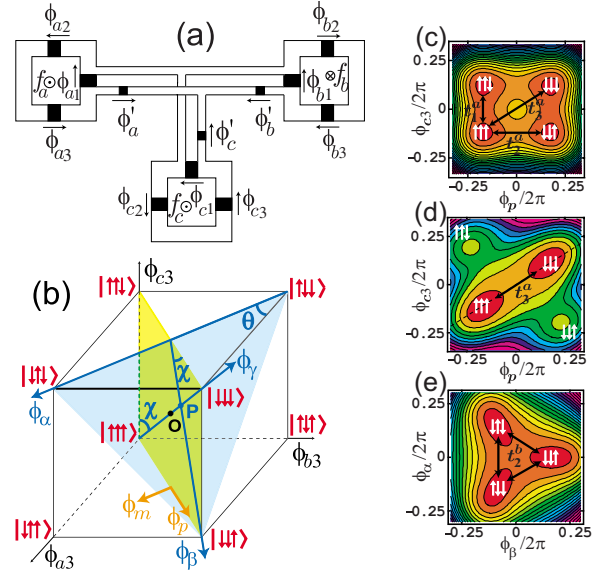


FIG. 1. (Color online) (a) A three flux qubit system. The black squares are the Josephson junctions. The Josephson coupling energies of the Josephson junctions in the qubit and connecting loop are E_{Ji} and E'_j , respectively. f_q 's are the external fluxes and ϕ 's are the phase differences across the junctions. (b) The eight states of three qubits are represented in $(\phi_{a3}, \phi_{b3}, \phi_{c3})$ space at the coresonance point. $(\phi_\alpha, \phi_\beta, \phi_\gamma)$ are the rotated coordinates and $O(0, 0, 0)$ is the origin of both coordinates. The blue (light gray) triangle intersects vertically the ϕ_γ axis at point P . For $E_{J1}/E_J = 0.7$, the effective potentials U_{eff} in (ϕ_p, ϕ_m) plane [yellow (dark gray) square in (b)] are plotted for (c) $E'_j = 0$ and (d) $E'_j/E_J = 0.5$. The dotted line in (d) coincides with ϕ_γ axis in (b). (e) The effective potential U_{eff} in $(\phi_\alpha, \phi_\beta)$ plane [blue (light gray) triangle in (b)] for $E'_j/E_J = 0.05$ and $E_{J1}/E_J = 0.75$. Here and after, the superscript a (in $t_i^{a(b)}$) denotes the tunneling processes including (excluding) the states, $|\uparrow\uparrow\uparrow\rangle$ or $|\downarrow\downarrow\downarrow\rangle$, and $i = 1, 2, 3$, the single-, two-, and three-qubit tunneling processes, respectively.

$= |c_1 c_6 - c_2 c_5|^2 + |c_1 c_7 - c_3 c_5|^2 + |c_1 c_8 - c_4 c_5|^2 + |c_2 c_7 - c_3 c_6|^2 + |c_2 c_8 - c_4 c_6|^2 + |c_3 c_8 - c_4 c_7|^2$ and $D_2(|\Psi\rangle)$ and $D_3(|\Psi\rangle)$ are obtained by exchanging the indices as $3 \leftrightarrow 5$ and $4 \leftrightarrow 6$ for D_2 and $2 \leftrightarrow 5$ and $4 \leftrightarrow 7$ for D_3 . For the GHZ state, $Q(|\Psi_{\text{GHZ}}\rangle) = 1$ and for the W state $Q(|\Psi_W\rangle) = 8/9$.

We plot the Q factors for the ground state in Figs. 2(a) and 2(b) as a function of the rotated fluxes $f_\alpha \equiv (f_a - f_b)/\sqrt{2}$, $f_\beta \equiv (f_a + f_b - 2f_c)/\sqrt{6}$, and $f_\gamma \equiv (f_a + f_b + f_c)/\sqrt{3}$. Note that the coresonance point $(f_a, f_b, f_c) = (1/2, 1/2, 1/2)$ is transformed to $(f_\alpha, f_\beta, f_\gamma) = (0, 0, \sqrt{3}/2)$. For $E'_j/E_J = 0.02$ in Fig. 2(a), $Q < 1$. However, as E'_j increases, the GHZ state appears around the coresonance point in Fig. 2(b). Figure 2(c) is the cut view of Q factor for various coupling strength. It is found that for the GHZ state, E'_j should be larger than $0.03E_J$. It turns out that the coupling strength from the inductive coupling scheme corresponds to $E'_j \approx 0.005E_J$.¹⁵ This shows that the inductive coupling scheme cannot provide a sufficient coupling for the GHZ state.

To be observed experimentally, the GHZ state should be robust against fluctuations of external flux. Figure 2(b) shows that the GHZ state can be obtained for a broad range of f_α and f_β . Thus, let us examine the behavior of Q factor as a function of f_γ [Fig. 2(d)]. If the peak width is too narrow

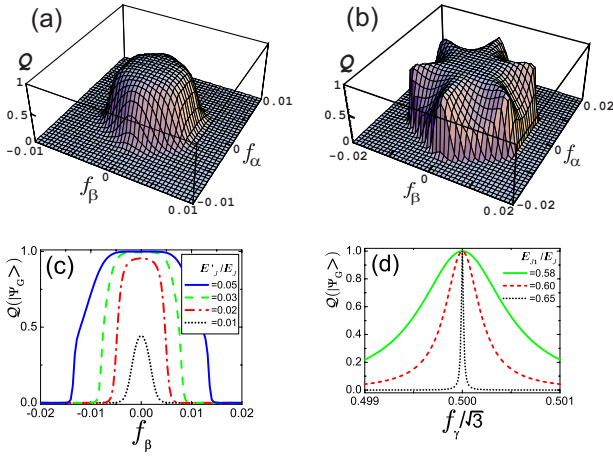


FIG. 2. (Color online) The Q factors of the ground state in the three qubit system for (a) $E'_j/E_j=0.02$ and for (b) $E'_j/E_j=0.05$. Here, $f_\gamma=\sqrt{3}/2$ and $E_{J1}/E_J=0.7$. (c) Cut view of Q factors in (a) and (b) for $f_\alpha=0$. (d) For $f_\alpha=f_\beta=0$ and $E'_j/E_j=0.6$, Q factors are plotted as a function of f_γ for several E_{J1} .

compared with the fluctuations of external flux, the GHZ state cannot be observed experimentally. Actually, it is found that the three-qubit tunneling t_3^a plays an important role for wide peak width. If other tunneling processes except t_3^a are negligible, small flux fluctuations can influence the Q factor given approximately by $Q(|\Psi\rangle)\approx(t_3^a)^2/[(\delta E)^2+(t_3^a)^2]$, where δE is the energy level change with $E_{\downarrow\downarrow\downarrow}=E_g+\delta E$ and $E_{\uparrow\uparrow\uparrow}=E_g-\delta E$, E_g the ground state energy, and $\delta E\propto(f_\gamma/\sqrt{3}-0.5)$.¹⁵ Qualitatively, then t_3^a corresponds to the peak width of the envelope of Q factor in Fig. 2(d). Consequently, the stronger t_3^a , the wider the range for the GHZ state.

However, the single-qubit tunneling t_1^a makes the coupled qubits unentangled. Thus, we need to suppress the single-qubit tunneling, while enhancing the three-qubit tunneling. In order to do so, we need strong coupling, as shown in Fig. 1(d), where the single-qubit tunnelings between the ground and excited levels become suppressed. On the other hand, the relevant parameter for t_3^a is the Josephson coupling energy E_{J1} . As E_{J1} decreases, the barrier in the double-well potential in Fig. 1(d) becomes lower. It implies that to get a larger value of t_3^a , E_{J1} should be smaller. However, too small E_{J1} makes some excited states $|s_a s_b s_c\rangle$ unstable. We show the minimum E_{J1} 's in Table I for three representative E'_j 's. In fact, we found that for strong coupling case, the excited states are stable for smaller E_{J1} . For small $E'_j/E_j=0.05$, we obtained $t_1^a/E_J=1.3\times 10^{-3}$ and thus $t_3^a/t_1^a\approx 5.4\times 10^{-3}$. How-

TABLE I. Peak widths for Q factors of GHZ state in Fig. 2(d) and of W state in Fig. 3(d) at 95% of the maximum values. Here, the unit of E'_j , E_{J1} , and t is E_J .

E'_j	E_{J1}	t_3^a	Peak width GHZ (δf_γ)	t_2^b	Peak width W (δf_α)
0.05	0.7	7.0×10^{-6}	$\sim 5\times 10^{-7}$	6.3×10^{-4}	$\sim 10^{-4}$
0.1	0.75	2.6×10^{-7}	$\sim 2\times 10^{-8}$	1.0×10^{-4}	$\sim 2\times 10^{-5}$
0.6	0.58	5.1×10^{-3}	$\sim 4\times 10^{-4}$	0	0

ever, for larger value of $E'_j/E_j=0.6$, we obtained $t_3^a/t_1^a\approx 6.4$ with $t_1^a/E_J=8.0\times 10^{-4}$. Hence, for the strong coupling case, we can expect higher Q factor for the GHZ state.

In Table I, the peak widths for both GHZ and W states are calculated at 95% of the maximum value of Q factor, which are approximately proportional to t_3^a and t_2^b , respectively. During the Rabi oscillations, the fluctuation of flux is estimated to be in the order of $10^{-6}\Phi_0/Hz^{1/2}$ (Ref. 24) and $1/f$ critical current fluctuations of the Josephson junctions is rather weak. In recent experiments for flux qubits, the flux amplitudes are controlled up to the accuracy of $10^{-5}\Phi_0$. In this respect, the peak width, $\delta f_\gamma\sim 4\times 10^{-4}$, for $E'_j=0.6E_J$ will be sufficient to observe the GHZ state experimentally.

In Fig. 1(b), we present the blue (light gray) triangle whose corners correspond to the three states consisting of the W state, $|\Psi_W\rangle=(|\uparrow\downarrow\downarrow\rangle+|\downarrow\uparrow\downarrow\rangle+|\downarrow\downarrow\uparrow\rangle)/\sqrt{3}$. The blue (light gray) triangle intersects ϕ_γ axis at $\phi_\gamma>0$. Actually, there is another intersection plane with $\phi_\gamma<0$ for another possible W state. For simplicity, we will focus on the W state on the blue (light gray) triangle plane. The effective potential at the plane of the blue (light gray) triangle for the three states is drawn in Fig. 1(e). Energetically, in our model, the energies of three states are higher than those of the two states consisting of the GHZ state, i.e., the ground state. Then, the W state can be observed in an excited state.

Let us discuss how a W state can be realized in an excited state. At the coresonance point $(f_\alpha, f_\beta, f_\gamma)=(0, 0, \sqrt{3}/2)$, the six states except for $\{|\downarrow\downarrow\downarrow\rangle, |\uparrow\uparrow\uparrow\rangle\}$ are degenerated in the second excited state. The six states are classified into two classes, $\{|\uparrow\uparrow\downarrow\rangle, |\uparrow\downarrow\uparrow\rangle, |\downarrow\uparrow\uparrow\rangle\}$ with $S_z=1/2$ and $\{|\downarrow\downarrow\downarrow\rangle, |\downarrow\downarrow\uparrow\rangle, |\downarrow\uparrow\downarrow\rangle\}$ with $S_z=-1/2$. Hence, the two classes of the six states can be separated by applying an additional flux Δf_γ . The three states of each class can form a W state. As shown in Fig. 1(e), the two-qubit tunneling amplitude t_2^b creates the W state, while the single-qubit tunneling t_1^b destroys the W state because it induces a superposition of states of the two classes. If other small tunnelings are negligible, then the Q factor is given by $Q(|\Psi\rangle)\approx 8[1+2.5(t_1^b/\Delta E)^2]/9\times[1+4(t_2^b/\Delta E)^2]$. From $Q(|\Psi_W\rangle)=8/9$, it turns out that $|\Delta E|\propto|f_\gamma/\sqrt{3}-1/2|$ should be much larger than t_1^b . Therefore, a sufficient Δf_γ is needed to generate a W state. Actually, we found that $|\Delta f_\gamma|\geq 0.01$ is sufficient to show the generation of a W state [Figs. 3(a) and 3(b)]. In Fig. 3(b), the W state is formed slightly away from the point, $f_\alpha=f_\beta=0$. For a relatively weak coupling, the single-qubit tunneling t_1^b , as well as t_2^b , becomes larger. Thus, an additional small flux $f_\beta\approx 0.0004$ will break the symmetry so that the state $|\Psi\rangle$ closer to the W state would be formed. In Fig. 3(c), we can see the W state around $f_\alpha=0$.

On the contrary to the GHZ state where the range of f_γ is critical for experimental observation, for W state the range in (f_α, f_β) plane is important, as shown in Figs. 3(a) and 3(b). Figure 3(d) shows the Q factor for W states whose peak widths depend on the value of the two-qubit tunneling amplitude t_2^b (Table I). As E'_j decreases, t_2^b becomes larger. However, if the coupling strength becomes too weak, the two classes with $S_z=\pm 1/2$ will become overlapped with each other through the single qubit tunneling t_1^b so that the W state may readily be broken. Hence, as a consequence of compromise, the W state emerges for an intermediate coupling

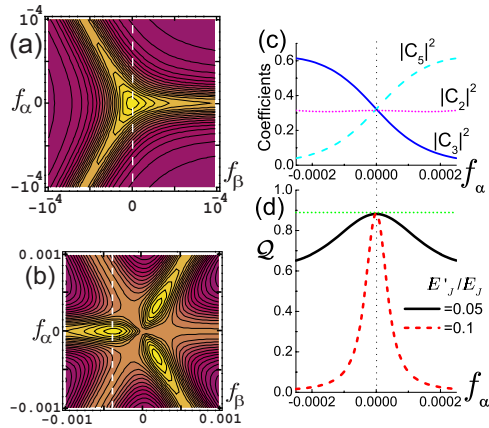


FIG. 3. (Color online) The Q factors of the second excited state with $f_\gamma = \sqrt{3}/2 - 0.01$ for (a) $E'_j/E_j = 0.1$ and $E_{j1}/E_j = 0.75$ and (b) $E'_j/E_j = 0.05$ and $E_{j1}/E_j = 0.7$. Note the different scales and positions of maximum Q factor in both figures. Here, the yellow (light gray) regions denote high Q factors. (c) The coefficients of the eigenstate used in (b) are plotted along the dotted line with $f_\beta = -0.0004$, which shows that W state is formed around $f_\alpha = 0$. (d) Cut view of Q factors along dotted lines in (a) and (b). The green dotted line indicates $Q = 8/9$ for W state. The peak width for $E'_j/E_j = 0.05$ is much wider than that for $E'_j/E_j = 0.1$.

strength, $E'_j = 0.05E_j$, with rather broader peak width, as shown in Table I.

The quantification of entanglement can be done by using the state tomography measurement.^{9,25} Recently, for capacitively coupled phase qubits, the tomography measurement has been done,⁹ where they simultaneously measure the state

of coupled qubits. For present coupling, we expect that the similar tomography measurement can also be performed.

The tripartite entanglement with superconducting qubits has not yet been achieved so far. For the bipartite entanglement, capacitively coupled phase qubits showed high fidelity in a recent experiment,⁹ while for charge qubits, only partial entanglement was observed. The interactions between phase qubits are XY -type interactions, which describe simultaneous two-qubit flipping processes. The two- or multiple-qubit tunneling processes are essential for entanglement of qubits.¹² However, for charge qubits, the interaction is mainly Ising type. We believe that this is the reason for weak entanglement in experiments with charge qubits. For three coupled phase qubits, the lowest energy state is $|000\rangle$ state, while the highest is $|111\rangle$ state. Hence, the superposition between these two states will be negligibly weak, thus the GHZ state cannot be formed. However, since the other states, for example, $|100\rangle$, $|010\rangle$, $|001\rangle$ states, are energetically degenerated, the W state could be obtained.

In summary, we investigate a three superconducting flux qubit system. The GHZ and W states can be realizable in the eigenstates of the macroscopic quantum system. We show that while the GHZ state needs strong coupling strength, the W state can be formed at an optimized coupling strength. Moreover, to keep the tripartite entangled states robust against external flux fluctuations for feasible experimental realizations, the three coupled qubit system can provide relatively large three-qubit and two-qubit tunneling amplitudes for GHZ and W states, respectively.

S.Y.C. acknowledges the support from the Australian Research Council.

*mdkim@kias.re.kr

†sycho@cqu.edu.cn

- ¹D. M. Greenberger, M. A. Horne, and A. Zeilinger, in *Bells Theorem, Quantum Theory, and Conceptions of the Universe*, edited by M. Kafatos (Kluwer Academic, Dordrecht, 1989).
- ²A. Zeilinger, M. A. Horne, and D. M. Greenberger, in *Proceedings of the Workshop on Squeezed States and Quantum Uncertainty*, edited by D. Han, Y. S. Kim, and W. W. Zachary (NASA, Washington, DC, 1992).
- ³W. Dür, G. Vidal, and J. I. Cirac, *Phys. Rev. A* **62**, 062314 (2000).
- ⁴A. Rauschenbeutel, *et al.*, *Science* **288**, 2024 (2000).
- ⁵D. Bouwmeester *et al.*, *Phys. Rev. Lett.* **82**, 1345 (1999); J.-W. Pan *et al.*, *Nature (London)* **403**, 515 (2000); J.-W. Pan *et al.*, *Phys. Rev. Lett.* **86**, 4435 (2001); M. Eibl *et al.*, *ibid.* **92**, 077901 (2004).
- ⁶C. F. Roos *et al.*, *Science* **304**, 1478 (2004); D. Leibfried *et al.*, *ibid.* **304**, 1476 (2004).
- ⁷Yu. A. Pashkin *et al.*, *Nature (London)* **421**, 823 (2003); T. Yamamoto *et al.*, *Nature (London)* **425**, 941 (2003).
- ⁸A. J. Berkley *et al.*, *Science* **300**, 1548 (2003).
- ⁹M. Steffen *et al.*, *Science* **313**, 1423 (2006); R. McDermott *et al.*, *ibid.* **307**, 1299 (2005).
- ¹⁰A. Izmailkov *et al.*, *Phys. Rev. Lett.* **93**, 037003 (2004); A. O. Niskanen *et al.*, *Science* **316**, 723 (2007).

¹¹J. H. Plantenberg *et al.*, *Nature (London)* **447**, 836 (2007).

¹²M. D. Kim and S. Y. Cho, *Phys. Rev. B* **75**, 134514 (2007).

¹³L. F. Wei, Y.-x. Liu, and F. Nori, *Phys. Rev. Lett.* **96**, 246803 (2006).

¹⁴J. B. Majer *et al.*, *Phys. Rev. Lett.* **94**, 090501 (2005).

¹⁵M. D. Kim and J. Hong, *Phys. Rev. B* **70**, 184525 (2004).

¹⁶M. Grajcar *et al.*, *Phys. Rev. B* **74**, 172505 (2006).

¹⁷M. D. Kim, *Phys. Rev. B* **74**, 184501 (2006).

¹⁸S. H. W. van der Ploeg *et al.*, *Phys. Rev. Lett.* **98**, 057004 (2007).

¹⁹S. Y. Cho and M. D. Kim, arXiv:cond-mat/0703505 (unpublished).

²⁰J. E. Mooij *et al.*, *Science* **285**, 1036 (1999); Caspar H. van der Wal *et al.*, *ibid.* **290**, 773 (2000); I. Chiorescu *et al.*, *ibid.* **299**, 1869 (2003); I. Chiorescu *et al.*, *Nature (London)* **431**, 159 (2004); T. Hime *et al.*, *Science* **314**, 1427 (2006).

²¹T. P. Orlando *et al.*, *Phys. Rev. B* **60**, 15398 (1999).

²²M. D. Kim, D. Shin, and J. Hong, *Phys. Rev. B* **68**, 134513 (2003).

²³D. A. Meyer and N. R. Wallach, *J. Math. Phys.* **43**, 4273 (2002).

²⁴F. Yoshihara *et al.*, *Phys. Rev. Lett.* **97**, 167001 (2006); P. Bertet *et al.*, *ibid.* **95**, 257002 (2005).

²⁵Y.-x. Liu, L. F. Wei, and F. Nori, *Phys. Rev. B* **72**, 014547 (2005).